Monthly Notices
of the
ROYAL ASTRONOMICAL SOCIETY

MNRAS **474,** 1572–1582 (2018)
Advance Access publication 2017 November 8

doi:10.1093/mnras/stx2881

The detection of discrete cyclotron emission features in phase-resolved optical spectroscopy of V1500 Cygni

Thomas E. Harrison[1]★ and Ryan K. Campbell[2]

[1]*Department of Astronomy, New Mexico State University, PO Box 30001, MSC 4500, Las Cruces, NM 88003-8001, USA*
[2]*Department of Physics and Astronomy, Humboldt State University, 1 Harpst St., Arcata, CA 95521, USA*

Accepted 2017 November 3. Received 2017 October 30; in original form 2017 September 12

ABSTRACT

We have obtained phase-resolved optical spectroscopy of the old nova and asynchronous polar V1500 Cyg. These new data reveal discrete cyclotron humps from two different strength magnetic fields. One region has $B = 72$ MG, while the other has $B \simeq 105$ MG. With the detection of these features, we revisit the optical/near-infrared light curves presented in Harrison & Campbell, and find that the large photometric excesses observed in those data are fully reconcilable with cyclotron emission. These results, when combined with the X-ray observations that appeared to have maxima that repeated on the orbital period, imply that V1500 Cyg has reverted back to a synchronous polar. Using existing theory, we show that the strong field strengths found here can explain the rapid spin-down time.

Key words: stars: individual: V1500 Cygni – novae, cataclysmic variables – infrared: stars – X-rays: stars.

1 INTRODUCTION

If there was a pantheon for classical novae, V1500 Cygni (Nova Cyg 1975) would almost certainly occupy the central altar. It was one of the brightest, fastest and most luminous classical novae (CNe) of all time. In the weeks before the eruption, the progenitor brightened by ∼7 mag, unique among CNe (Collazzi et al. 2009). Stockman, Schmidt & Lamb (1988) found that the light from V1500 Cyg was circularly polarized, indicating a highly magnetic system. It was a 'polar'. Strangely, the period of the sinusoidal variation in the circular polarization was not synchronized to the orbital period, but to a period that was 2 per cent shorter. Unlike all other polars known at the time, the white dwarf in V1500 Cyg was spinning with a period that was different from the orbital period. Apparently, the CN eruption had knocked the system out of synchronism, and V1500 Cyg became the first identified 'asynchronous polar'. Nearly as surprising was the finding that the white dwarf spin period was lengthening, and the system would again attain synchrony within ∼200 yr (Schmidt & Stockman 1991).

To attempt to explain the rapid spin-down time-scale of V1500 Cyg and other asynchronous polars, Campbell & Schwope (1999) developed a model that used the torque resulting from induced electric fields and current flow in the secondary star from an asynchronously spinning magnetic white dwarf to slow its rotation rate. In their modelling, if the white dwarf mass was of the order of 0.5 $M_{\odot}$, the spin-down time-scale was of the order of 50 yr. If the white dwarf mass was higher than this, the spin-down time-scale would be longer. Given the violence of the CN eruption of V1500 Cyg, and the presence of a modest enhancement of neon in its ejecta, it is assumed that the mass of the white dwarf in V1500 Cyg is large (Lance, McCall & Uomoto 1988; Politano et al. 1995). Since the spin-down time-scale is directly proportional to the mass of the white dwarf, the time required to attain synchrony would be of the order of ∼100 yr. To agree with the observations of Schmidt & Stockman (1991) simply requires the white dwarf to have a magnetic field strength that is of the order of $B \sim 28$ MG.

Harrison & Campbell (2016, hereafter 'HC16') obtained *XMM–Newton* observations of V1500 Cyg that showed a strong X-ray maximum once each orbit. Timing analysis of the five observed maxima in this light curve appeared to suggest that the white dwarf was now spinning at the orbital period – the system had become synchronized. This conclusion was supported by optical and infrared light curves that, while dominated by flux from the heavily irradiated secondary star, appeared to show excesses that always occurred at the same orbital phases. These data spanned 7 yr, and suggested that the system had attained synchrony as early as 2007. HC16 attributed the largest of these excesses to cyclotron emission from a pole with a magnetic field strength of ≈80 MG. This high magnetic field strength could explain the rapid spin-down rate using the Campbell & Schwope prescription. For a field strength near 80 MG, the $n = 2$, 3 and 4 cyclotron harmonics would be present in optical spectroscopy.

These results suggest that it should be feasible to detect discrete cyclotron harmonic emission in the spectra of V1500 Cyg. We have obtained phase-resolved optical spectroscopy and find that the spectra of V1500 Cyg do exhibit cyclotron emission features throughout its orbit. We have attempted to model those features to estimate the parameters of the cyclotron emission regions. The phases at which the cyclotron emission occurs have led to a complete

★ E-mail: tharriso@nmsu.edu

revision of the light-curve modelling presented in HC16. In the next section, we discuss the data set, in Section 3 we present the new phase-resolved spectra and model it, and the light-curve data from HC16. We discuss these results in Section 4, and present our conclusions in Section 5.

2 DATA

Observations of V1500 Cyg were obtained on 2017 July 17 using the Double Imaging Spectrograph[1] (DIS) on the Apache Point Observatory 3.5 m. The two channels of DIS allow simultaneous optical spectra in both the blue and the red, by using a dichroic mirror with a transition wavelength of 5350 Å. This creates two separate optical paths feeding separate gratings. The default low-resolution mode was used, delivering a dispersion of 1.8 Å pixel^{-1} in the blue and 2.29 Å pixel^{-1} in the red. The target was observed from 07:17 to 10:51 UT, covering a full orbit ($P_{\rm orb} = 3.35$ h). The exposure times for V1500 Cyg were all identical, 720 s. In the following, we have used the minimum light ephemeris of Semeniuk, Olech & Nalezyty (1995) to calculate the phases of our data set. As described below, the phasing of this ephemeris does not correspond to inferior conjunction of the secondary, but to the time of the *V*-band minimum. As shown in HC16, the light curves in the *BVRIJHK* bandpasses all have minima *near* $\phi = 0.0$. The maximum error in the Semeniuk et al. ephemeris, which has a T0 date of 1986 September, at the epoch of our spectroscopic data set is $\Delta\phi = \pm 0.13$.

The data were reduced in the usual fashion using IRAF. In addition, however, the techniques outlined by Bessell (1999), to use a 'smooth star' to correct for telluric features in optical spectra, were also applied to these data to aid in the identification of any weak cyclotron features. The white dwarf L1363-3 was observed immediately after finishing the observations of V1500 Cyg. It was used to both remove the telluric features and to correct for any residuals that remained from the flux calibration process. As shown in Fig. 1 for one of our spectrophotometric calibrators for the V1500 Cyg data set, HR 9087, this technique yielded excellent results, with only small residuals in the Fraunhofer *A* band (λ7600 Å). We also locate the dichroic transition wavelength in Fig. 1. A residual exists at this wavelength in all of the DIS spectra, and becomes somewhat more substantial for fainter sources like V1500 Cyg. A small region around this location has been omitted from the plots of the DIS spectra for V1500 Cyg. The raw spectra at $\phi = 0.17$ have S/N = 13 in the continuum at both 5000 and 6000 Å.

3 RESULTS

The analysis of the *XMM* data for V1500 Cyg in HC16 indicated that the spin period of the white dwarf was very close to that of the orbital period. Unfortunately, the X-ray maxima of V1500 Cyg are quite variable, and the *XMM* observations were too short to confidently confirm synchronization. The compilation of optical/IR light curves presented in HC16 spanned some 7 yr. Over that time period, the phasing and morphology of the light curves did not change. One could overlay the 2006 July 12 *JHK* data on top of the 30 October 2014 photometry, and they would be nearly indistinguishable. A similar result is found for the visual photometry, though V1500 Cyg exhibits larger variability at shorter wavelengths. It is not obvious how the excesses observed in the *BVRIJHK* light curves could originate from the secondary star. Thus, they must come from a source associated with the white dwarf or the accretion stream. HC16 concluded that they were due to cyclotron emission from a synchronously rotating white dwarf.

The analysis of the X-ray data found two maxima. In the frame of the Semeniuk et al. ephemeris, the stronger of these occurred at $\phi = 0.82$, with a secondary maximum occurring at $\phi = 0.32$. HC16 modelled the X-ray light curve with two spots, with the primary accretion region on the white dwarf located below the line of sight. This meant that it was visible for less than one half of an orbital period. Due to its much lower luminosity, the location of the secondary accretion region was not well constrained. They simply placed it opposite to the primary region following the results of Stockman et al. (1988), who concluded that the two accretion regions responsible for the observed polarization were on opposite sides of the white dwarf. Being in the upper hemisphere ensures that the secondary pole remains visible for a longer time interval than the primary pole.

3.1 The orbital evolution of the spectra

We present the phase-resolved spectra in four panels in Fig. 2. All of the spectra for V1500 Cyg have been dereddened using the 'deredden' task in IRAF assuming $A_{\rm V} = 1.2$. The deredden task employs the reddening law of Cardelli, Clayton & Mathis (1989). Lance et al. (1988) have compiled published values for the extinction to V1500 Cyg, and the majority of them have $A_{\rm V} = 1.4$. During the cyclotron modelling discussed in the next section (the coloured lines in Fig. 2), we found that an extinction of $A_{\rm V} = 1.4$ mag produced a continuum that was too blue for us to match with any model that was comprised of a hot white dwarf, an irradiated (cool) secondary star and a cyclotron component. This may be due to our naïve assumptions about the underlying source, but models matched to the data dereddened by $A_{\rm V} = 1.2$ mag appeared to produce sensible results with the minimum number of spectral components.

The first panel, Fig. 2(a), presents the spectra in the interval $0.17 \leq \phi \leq 0.36$. A single broad hump, centred near 5400 Å, is present in each of the four spectra. As the system slowly brightens towards visual maximum ($\phi = 0.5$), the symmetric hump grows to its largest size at $\phi = 0.23$, and then declines to become much weaker by $\phi = 0.36$. During the phase interval presented in Fig. 2(a), the H I and He I emission lines are at their strongest, indicating that they might be partially due to irradiation of the donor star. In the phase interval $0.43 \leq \phi \leq 0.55$, Fig. 2(b), the hump remains relatively unchanged, though with a subtle shift in its peak to a longer wavelength at $\phi = 0.55$. By $\phi = 0.62$, the hump is very weak, and appears to be narrower. Over the interval $\phi = 0.68$ to 0.87, Fig. 2(c), the continuum undergoes dramatic changes with the addition of humps centred near ∼4000 and 7400 Å. At $\phi = 0.0$, Fig. 2(d), near the time of the light-curve minimum, the strongest hump seen in the preceding set of spectra is now considerably smaller, is more symmetric and appears to have shifted redwards. The phase 0 spectrum also appears to have features that are suggestive of a late-type star. In Fig. 3, we plot the red side of the $\phi = 0.0$ spectrum of V1500 Cyg, and compare it to that of the M5 dwarf Gl 866A (obtained using DIS).

The rapid change in the morphology and strength of the broad hump over an orbital period suggests that this feature can only be properly explained as due to cyclotron emission. As we describe below, we believe that there is actually cyclotron emission from two different regions with differing magnetic field strengths. It just happens that the peak fluxes from their strongest cyclotron harmonics occur at *similar* wavelengths. The fact that the cyclotron

[1] http://www.apo.nmsu.edu/arc35m/Instruments/DIS/

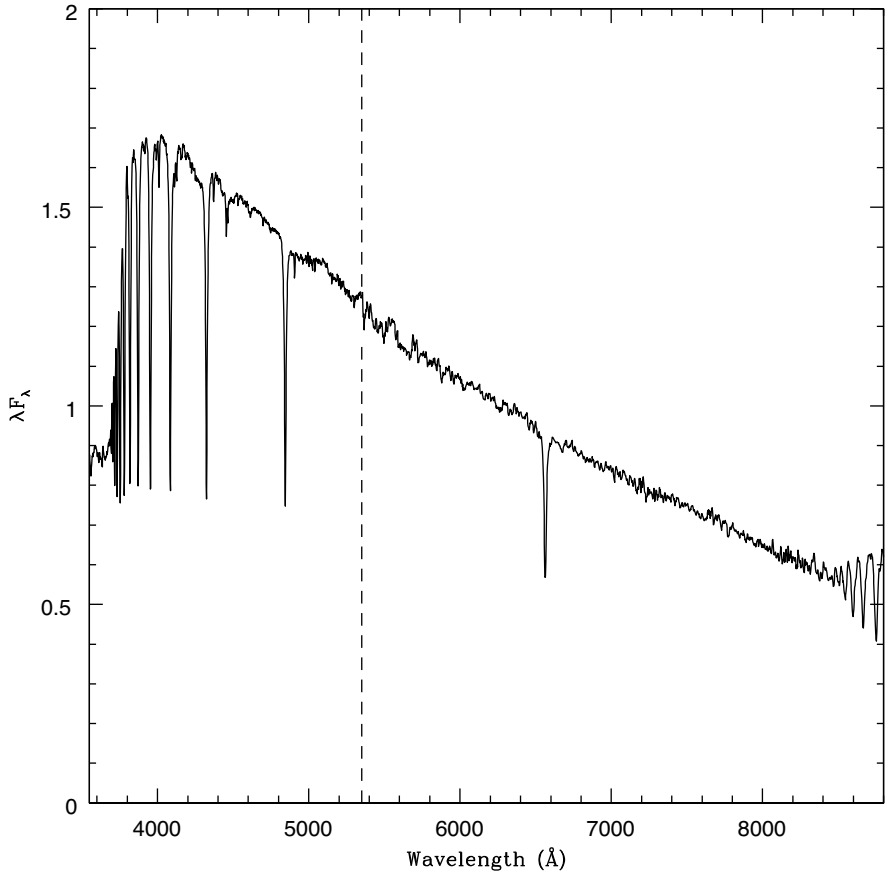

Figure 1. The spectrum of HR 9087 after correction by the 'smooth star' spectrum (see the text). The location of the transition wavelength for the dichroic in the DIS spectrograph is indicated by the vertical, dashed line.

emission features are strongest near $\phi = 0.85$ suggests that at this time, the origin of most/all of the cyclotron emission is associated with the primary accreting pole. The more symmetric hump, seen from $0.17 \leq \phi \leq 0.68$, is then associated with the secondary pole. There appears to be cyclotron emission at all phases of the orbit.

3.2 Cyclotron modelling

The appearance of a cyclotron emission spectrum depends on a variety of parameters. In the 'constant-Λ' modelling prescription (see Schwope 1990), these are the magnetic field strength (B), the temperature of the cyclotron emission region (kT), the viewing angle (θ) and the log of the optical depth parameter (Λ). To construct cyclotron models, we employ the constant-Λ code used by Campbell (2008), originally developed by Schwope (1990). The X-ray observations modelled in HC16 provide us with information on the temperatures of the two poles, with weaker constraints on the locations of the emission regions. For the primary X-ray emission region, for the two-component model they used (absorbed blackbody and free–free sources), a temperature for the thermal bremsstrahlung component of $kT = 40 \pm 9$ keV was found. Their fit for the much fainter secondary pole found $kT = 1.85 \pm 0.7$ keV. Given the low flux, the properties of this pole were not tightly constrained. The duration of the primary X-ray maximum indicated that the pole associated with this emission was visible for less than one half of an orbital period. HC16 located this pole at a co-latitude of $\beta_1 = 120^\circ$, placing it in the hemisphere that is below our line of sight. With the only constraint being the anti-phasing of the X-ray emission, the secondary pole was placed diametrically opposite to the primary pole giving $\beta_2 = 60^\circ$. With a binary inclination of $i \approx 60^\circ$ (Schmidt, Liebert & Stockman 1995), this region would be in view for more than one half of an orbit. For cyclotron modelling, such a co-latitude suggests that the viewing angle to the secondary pole changes very slowly over an orbit. The opposite is true for the primary pole, with larger viewing angles throughout its visibility. As discussed in HC16 (and references therein), low viewing angles to the emission region result in broader, less distinct cyclotron harmonics. Higher viewing angles produce narrower cyclotron emission features [for a much fuller discussion on how the parameters in a constant-Λ model influence the appearance of cyclotron spectra, see Harrison & Campbell (2015)].

As shown in Campbell (2008), synthetic spectra produced from constant-Λ modelling generally require orbitally (phase) dependent values for B, Λ and kT to match observations. Even if one has a relatively good understanding of the location of the cyclotron emission region, and of the underlying continuum source, the assumptions of a constant temperature accretion region, a single value of Λ or one magnetic field strength are never realized. It is also likely that the cyclotron emission region is not a point source, and a single value for θ or B is unrealistic. It is also easy to obtain similar solutions by simultaneously changing the values of just two parameters. For example, B and θ are partially degenerate. Constant-Λ models are also arbitrarily normalized. Thus, any solution that is derived from such modelling can only be assumed to be approximate, even when multiple harmonic features are observed. In the modelling

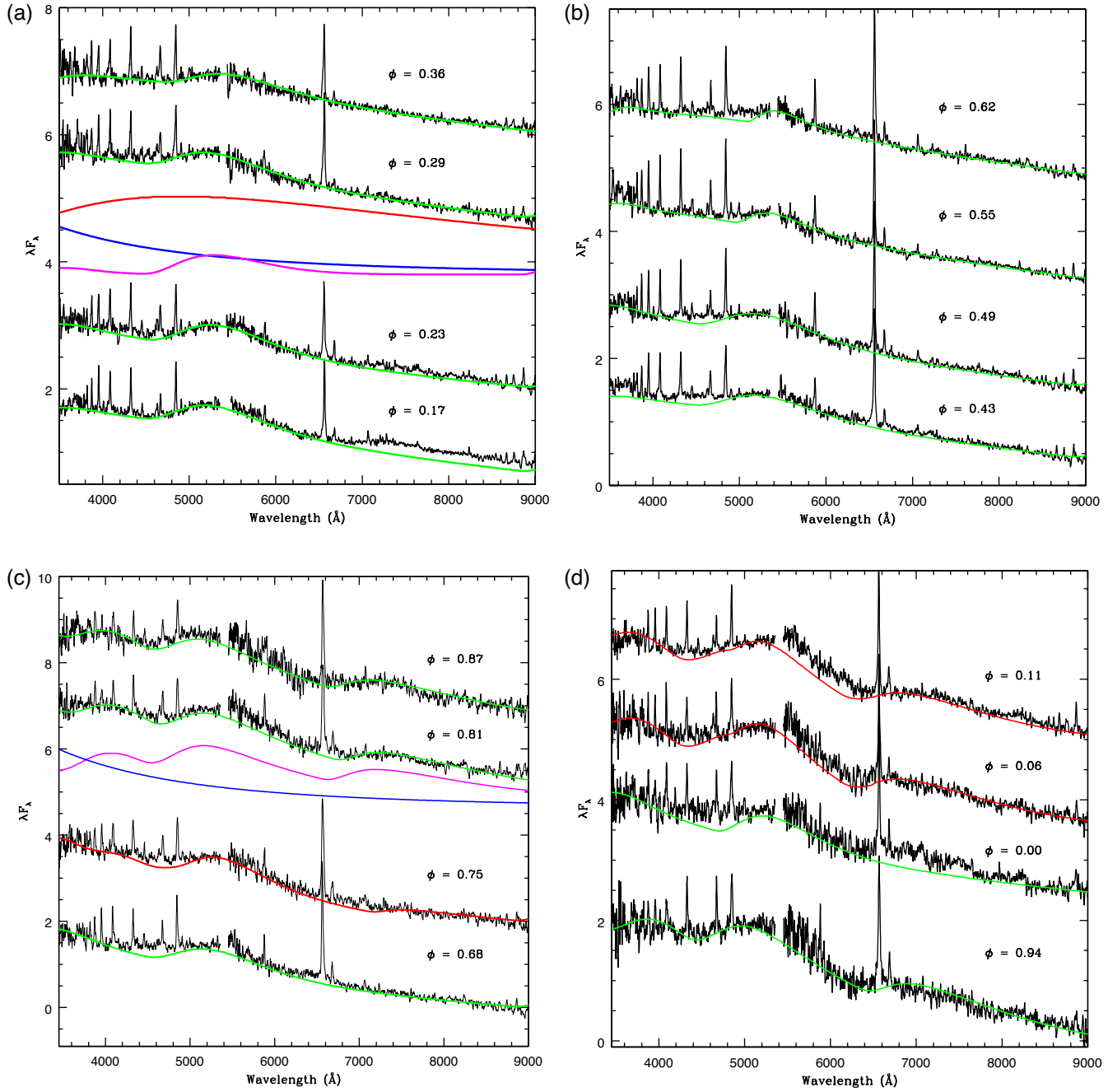

Figure 2. (a) The spectra (black) for the phase interval $0.17 \leq \phi \leq 0.36$. Models (see Section 3.2) have been fitted to the data (green). For the $\phi = 0.29$ spectrum, we plot the three spectral components that comprise our final model spectrum. This includes a hot blackbody source with $T_{\rm eff} = 54\ 000$ K (blue), the irradiated secondary star with $T_{\rm eff} = 6100$ K (red) and a cyclotron spectrum with $B = 105$ MG, $kT = 16$ keV, $\theta = 60^{\circ}$, $\log\Lambda = 0.0$ (magenta). The model spectra for the other phases in this plot have components with very similar parameters as those for $\phi = 0.29$. The spectra in this, and all figures that follow, have been boxcar smoothed by 5 pixels. They have also been vertically offset by arbitrary values for clarity. See Fig. 4 for approximate *UBVRI* fluxes. As in panel (a), but for the phase interval $0.43 \leq \phi \leq 0.62$. (c) The spectra for the phase interval $0.68 \leq \phi \leq 0.87$. The cyclotron model for $\phi = 0.68$ has $B = 105$ MG (secondary pole), while those for $\phi = 0.81$ and 0.87 have $B = 72$ (primary pole). The model for $\phi = 0.75$ (red) results from combining cyclotron models with both of these field strengths. The cyclotron emission at this phase is dominated by that from the 105 MG pole. We plot the relative contributions of the hot white dwarf (blue), and a cyclotron model with $B = 72$ MG, $\theta = 60^{\circ}$, $kT = 35$ keV, $\log\Lambda = 1.6$ (magenta) for the model (green) of the $\phi = 0.81$ data set. (d) The spectra of V1500 Cyg covering the phase interval $0.94 \leq \phi \leq 0.11$. The green curves are one-component cyclotron models. The model for $\phi = 0.94$ has $B = 72$ MG, while that for $\phi = 0$ has $B = 105$. Cyclotron models that result from a combination of these field strengths are plotted in red.

described below, the uncertainty about the orbitally evolving continuum source, and our inability to constrain the location of the secondary pole, leads to additional difficulties in characterizing the cyclotron emission.

We start by modelling the spectra near $\phi = 0.25$ (Fig. 2a), as there is a single, symmetric hump at this time. HC16 modelled the *BVRIJHK* light curves with two stellar components having temperatures of 52 000 and 3100 K. The exact value of the temperature for the

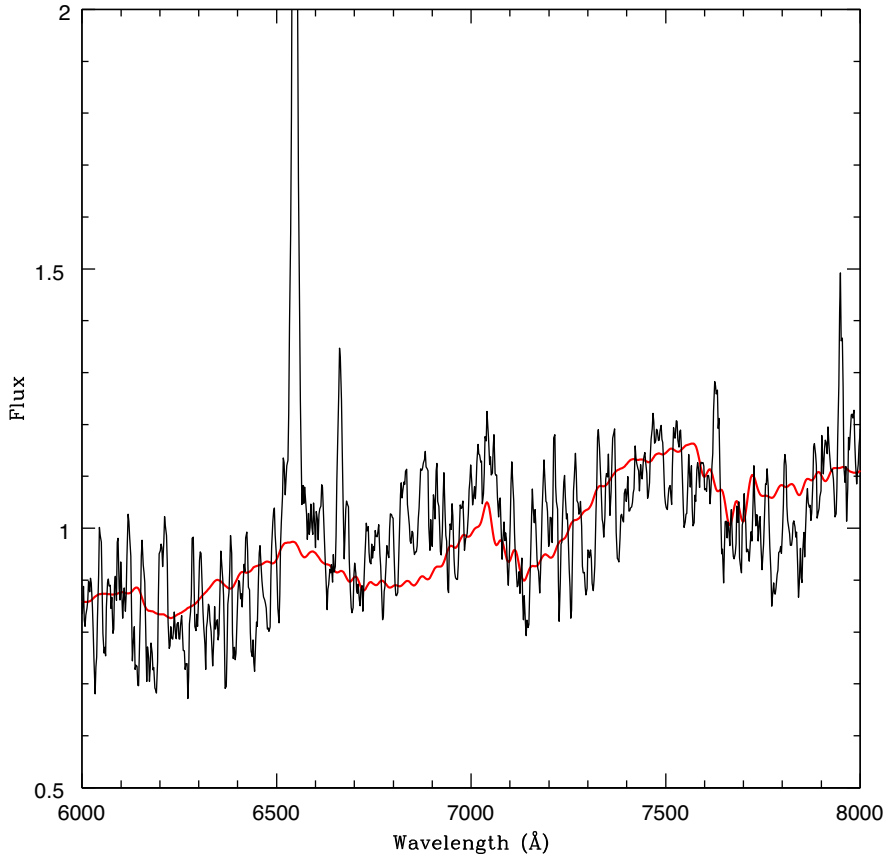

Figure 3. A comparison of the $\phi = 0$ spectrum of V1500 Cyg (black) to that of the M5 dwarf Gl 866A (red).

white dwarf is mostly irrelevant for the modelling here, since such a hot source peaks far into the UV, and only the tail of this source's spectrum is present in our data set. At superior conjunction, we estimate that the irradiated secondary has a temperature of the order of $T_{\rm eff} \simeq 6100$ K. Much of the rise to visual photometric maximum is due to the increased visibility of the donor's irradiated hemisphere. Thus, our models for the continuum of V1500 Cyg near $\phi = 0.25$ comprise two blackbodies, the hot white dwarf primary and the irradiated hemisphere of the secondary. We allowed the ratio of their contributions to be a variable at all times in this modelling. We discuss constraints on their relative luminosities in the next section. We also separately adjusted the strength of the cyclotron emission to best match each of the spectra.

We find that a cyclotron component with the following attributes explains all four spectra in Fig. 2(a): $B = 105$ MG, $kT = 16$ keV, $\theta = 60^\circ$ and $\log\Lambda = 0$. The cyclotron hump centred near $\lambda = 5400$ Å is the $n = 2$ harmonic for this field strength. The $n = 3$ harmonic would be centred near 3600 Å. The weakness of the $n = 3$ harmonic requires a low value for $\log\Lambda$. As discussed above, these phases are associated with the visibility of the secondary accretion region. If it originates from a point source, the broadness of the dominant cyclotron feature requires a temperature that is much higher than estimated from fitting its X-ray spectrum. We find that it is extremely difficult to reproduce the breadth of this feature with temperatures less than $kT \simeq 16$ keV. A similar quality of fit can be easily achieved with slightly higher temperatures by simultaneously changing the viewing angle and the field strength. At much higher temperatures, $kT > 20$ keV, the shape of the $n = 2$ harmonic becomes much more peaked on the blueward side and does not resemble the observed feature. In Fig. 2(a), we present a deconvolution of the final model used to explain the $\phi = 0.29$ spectrum.

Because these spectra cover the time of transit of this region ($\phi = 0.32$), the viewing angle to this pole is near a minimum at this phase. If $i = 60^\circ$ and $\beta_2 = 60^\circ$, then $\theta = 0^\circ$ at $\phi = 0.32$. There should be very little detectable cyclotron emission at this time. The fact that it is still detectable suggests that $\beta_2 < 60^\circ$ or that the cyclotron emission is offset from the magnetic pole. As discussed in Schmidt & Stockman (1991), the broad sinusoidal polarization maxima suggested large (or distributed) cyclotron emission regions. This could explain the limited change in the viewing angle found in the modelling above, as well as the fact that significant cyclotron emission remains present during the transit of the magnetic pole. A distributed cyclotron emission region would also lead to a broader harmonic from the superposition of emission from regions with slightly different field strengths and viewing angles. This might help explain the much hotter temperature we derive here, versus the X-ray results. Note that the spectrum at $\phi = 0.17$ appears to have a red excess above the model we have used to fit its cyclotron emission. We will find that in addition to emission from the $B = 105$ MG pole, cyclotron emission from the primary pole, with its lower strength field, is necessary to explain several of the spectra following the light-curve minimum near $\phi = 0.0$.

For the next phase interval, $0.43 \leq \phi \leq 0.62$ (Fig. 2b), the cyclotron hump becomes weaker and begins to change in shape. Given the fact that we only have a single well-defined cyclotron harmonic, we model the spectra at $\phi = 0.43$ and 0.49 using the same

parameters as used for the spectra in Fig. 2(a). While it is subtle, the peak in the cyclotron emission appears to shift redwards between $\phi = 0.49$ and 0.55. To fit the latter spectrum, we used the same basic model, but with a higher viewing angle: $\theta = 75^\circ$. A changing viewing angle to the magnetic pole shifts the location of the wavelength of peak emission of a cyclotron harmonic (cf. Schwope & Beuermann 1997). Finally, to fit the very small and poorly defined hump in the $\phi = 0.62$ spectrum, we used a model with the viewing angle increased to 85°. Such a high viewing angle is consistent with the expectation that this accreting pole is near the limb of the white dwarf at this phase. As we discuss in the next section, a small hotspot associated with the secondary pole would become self-eclipsed near $\phi = 0.71$.

The dramatic change in morphology of the spectra over the phase interval $0.68 \leq \phi \leq 0.87$ (Fig. 2c) indicates that a different cyclotron emission spectrum has emerged, one associated with the primary pole. We begin by modelling the spectrum at $\phi = 0.87$, as the distortions to the continuum are largest at this time. We find that a cyclotron model with $B = 72$ MG, $\theta = 62^\circ$, $kT = 35$ keV and $\log\Lambda = 1.6$ explains the data. The broadness of the humps requires a very high temperature, in agreement with the X-ray observations of the primary accretion region. The cyclotron feature that peaks near 5200 Å is the $n = 3$ harmonic for this field strength. The blue continuum shortwards of 4800 Å is well modelled by the $n = 4$ harmonic from this pole. The change in the slope of the continuum near 6500 Å is fitted by the $n = 2$ harmonic. At this phase, the cyclotron fundamental would peak near 1.35 μm.

A nearly identical model, but with $\theta = 60^\circ$, can be fitted to the $\phi = 0.81$ spectrum. This spectrum coincides with the transit of the primary pole, and the deconvolution of the model spectrum shown in Fig. 2(c) shows that it is comprised of just the combination of emission from a hot blackbody source (blue) and cyclotron emission (magenta). If the orbital inclination is 60° and $\beta_1 = 120^\circ$, the viewing angle should be $\theta = 60^\circ$. The presence of multiple harmonics in these spectra allows for more robust models to be constructed than was possible for the secondary pole. The $\phi = 0.75$ spectrum is unusual. The expectation is that it should be dominated by cyclotron emission from the primary pole. We could not find a model using only a cyclotron emission spectrum from the field with $B = 72$ MG that would reproduce this spectrum. The model (in red) is a composite of the $B = 105$ model used to explain the spectra at earlier phases and the $B = 72$ MG model used at later phases. This is amplified by the fit to the $\phi = 0.68$ spectrum, where *only* the $B = 105$ MG ($\theta = 60^\circ$, $kT = 16$ keV and $\log\Lambda = 0.0$) model was used.

Two of the spectra in Fig. 2(d) will require a similar two-component cyclotron model. However, the spectrum at $\phi = 0.94$ needs only emission from the lower field strength region: $B = 72$ MG, $\theta = 50^\circ$, $kT = 35$ keV and $\log\Lambda = 1.6$. What is confusing is that if we have the lowest viewing angle to the emission region at $\phi = 0.94$, the viewing angle to this pole at $\phi = 0.0$ should probably be similar. As shown in Fig. 2(d), we model the spectrum at $\phi = 0.0$ with a single-component cyclotron model, but with that from the $B = 105$ MG field! After $\phi = 0.0$, we see the return of emission from the cyclotron component with $B = 72$ MG, but now in combination with emission from the $B = 105$ MG pole. It is clear that emission from the $B = 72$ MG field is dominant in the spectra for $\phi = 0.06$ and 0.11, but the broadness of the peak at 5400 Å suggests that emission from the $B = 105$ MG pole is also contributing to the spectra at these phases. These results argue that the cyclotron emission from the lower strength field is not co-located with the primary X-ray pole.

3.3 Reconciliation of the cyclotron emission with the *UBVRI* light curves

In HC16, the standard interpretation for the *V*-band light curve of V1500 Cyg was employed, where the visual maximum that occurred at phase 0.5 was due solely to the irradiated secondary star. With this phasing, $\phi = 0$ would correspond to the inferior conjunction of the donor. If true, this leads to a large excess in the *BVRIJHK* light curves in the interval $0.0 \leq \phi \leq 0.4$ (see fig. 5 in HC16). HC16 found that they could not reconcile this large excess with cyclotron emission from either of the two X-ray poles without dramatically offsetting its location well away from the poles. The fact that there is strong cyclotron emission near the time of primary X-ray pole transit indicates that the absolute phasing of the underlying binary used in HC16 (and presumed elsewhere) is wrong.

Insight into the true phasing of the stellar components in V1500 Cyg can be drawn from the *JHK* light curves in HC16 (their fig. 7). The maximum in those light curves occurs at $\phi = 0.32$, exactly at the phase where the primary X-ray pole would be facing away from the observer. Given the high temperature of this source, it would help increase the irradiation of the donor, leading to a light-curve maximum. As we have just shown, there is cyclotron emission at all phases; thus, the exact phasing of the secondary in its orbit remains somewhat uncertain. Looking at the *K*-band light curve, perhaps the step stretching from $\phi = 0.4$ to 0.5 in these data actually arises from the irradiated secondary, and is not due to cyclotron emission. If so, it is possible that the secondary could lag the primary X-ray pole by as much as 0.10 in phase. We find that we are able to construct a more robust set of light-curve models with the assumption that inferior conjunction of the secondary star occurs near $\phi \simeq 0.82$. This change in perspective shifts the period of the largest observed excesses in the optical/IR light curves to the phase interval $0.7 \leq \phi < 1.0$, associating them with the visibility of the primary pole, and the period when the cyclotron features in the optical spectra are at their strongest.

Before we attempt to construct new models for the *UBVRIJHK* light curves of V1500 Cyg, we attempt to characterize the stellar components in the system. The light curves in HC16 (their fig. 6) have $V = 19.35$ at minimum light. The distances to CNe are difficult to estimate. Lance et al. adopted $d = 1.2$ kpc for V1500 Cyg from a variety of published values, while Slavin, O'Brien & Dunlop (1995) found $d = 1.5$ kpc from a nebular expansion parallax. If we use $d = 1.2$ kpc, we derive $M_V = 7.8$ at minimum light. Given that cyclotron emission is always present, this is the upper limit to the combined luminosity of the primary and secondary stars (plus any contribution from a hotspot). A normal M4V has $M_V = 12.71$ (Bessell 1991), while the Roche lobe filling secondary star of U Gem (spectrally classified as an M4, but see Harrison 2016) has $M_V \simeq 10.1$. At minimum light, the luminosity of V1500 Cyg is dominated by the white dwarf primary, since we are (mostly) viewing the unirradiated hemisphere of the secondary. White dwarfs that have absolute visual magnitudes near that of V1500 Cyg all have high temperatures, $T_{\rm eff} \sim 40\ 000$ K (Vennes et al. 1997). Though nearly all of those white dwarfs have lower masses ($M_{\rm wd} \leq 0.7$ M$_\odot$) than that expected for V1500 Cyg ($M_1 \gtrsim 1$ M$_\odot$; see HC16).

At the time of our best view of the irradiated hemisphere of the secondary star, $\phi \simeq 0.32$, V1500 Cyg has $V = 18.4$ or $M_V = 6.8$. Assuming that the white dwarf has the same *V*-band luminosity

at all phases implies that the irradiated secondary star has M_V = 7.3. The two stellar components supply somewhat similar fluxes at this phase. With an estimated radius of 0.42 $R_\odot$, the irradiated hemisphere of the donor star has $T_{\rm eff} \sim 5200$ K. The observed colour at this time is $(B-V) = 0.4$, and with $A_V = 1.2$, $(B-V)_0 = 0.0$. To arrive at this combined colour suggests that the white dwarf itself must have $(B-V)_0 \lesssim -0.4$, corresponding to a temperature in excess of 40 000 K (Cheselka et al. 1993). Again, there is cyclotron emission in the V bandpass at this phase, making such estimates highly uncertain. It appears that there is little cyclotron emission in the infrared at phases near maximum. At this time $(J-K)$ = 0.5 and, with $A_V = 1.2$, is consistent with an object that has $T_{\rm eff}$ = 6100 K.

In Fig. 4, we re-plot the *UBVRI* light curves of V1500 Cyg from HC16. Given the excellent observing conditions, we have extracted broad-band magnitudes from the new spectra to create light curves. Given the low S/N of the bluest portion of the spectra, the bandpass used to generate the '*U*-band' light curve only spans the wavelength interval from λ = 3656 to 3826 Å (versus λ3656 ± 170 Å for Johnson *U*). Due to the dichroic cutoff, the *V* bandpass, nominally 5450 ± 500 Å, had to be truncated at λ = 5200 Å. Thus, the light curves in these two bands only approximate the true *U*- and *V*-band fluxes. To normalize the data set in each band, we offset each of the light curves so that the flux that falls closest to that of the model light curves falls exactly on the light curves. For the *U* band, this occurred at $\phi = 0.87$. For all of the other bandpasses, this occurred at $\phi = 0.36$, near the time of the transit of the secondary pole. The similarity between the spectroscopic light curves and the photometric light curves is striking, while also highlighting changes in the apparent strength of the cyclotron emission.

We locate the phases of the pole transits with vertical lines (solid for the primary maximum and dashed for the secondary maximum) in Fig. 4. Presuming a synchronous system, we use the Wilson–Devinney code (WD2010[2]) to produce models, but now require the phase of the irradiation-induced maximum to occur at $\phi = 0.32$. For the model presented in Fig. 4, we assume a secondary star with $T_{\rm eff}$ = 3000 K and a binary inclination of $i = 60^\circ$. We then let the temperature of the white dwarf be a free parameter. In addition, we add a hotspot (with a size and temperature to be determined from the modelling) on the white dwarf located at the longitude that corresponds to the primary X-ray maximum. HC16 found that the primary X-ray region appears to be visible for about $\Delta\phi = 0.18$. As in that paper, we assume that the duration of this transit is due to the 'southerly' co-latitude of the accretion region. We find that $\beta_1 = 128^\circ$, versus $\beta_1 = 120^\circ$ derived in HC16, is more consistent with the light-curve data.

The most stringent requirement for modelling the light curves of V1500 Cyg is to reproduce the large-amplitude variations seen in the near-infrared (near-IR). This amplitude is almost completely due to the irradiation of the donor star, and thus is a sensitive measure of the temperature of the two stellar components in the system. To get a significant temperature change on the irradiated hemisphere of the donor requires it to have a cool temperature. Secondaries with $T_{\rm eff} \geq 4000$ K cannot produce the observed variations. Given the relatively short orbital period of V1500 Cyg, and the results in Fig. 3, we have chosen to fix the donor star temperature to $T_{\rm eff}$ = 3000 K. Hotter donor star temperatures will require hotter white dwarf temperatures to get the same response, while a cooler secondary star can be irradiated with a cooler white dwarf to recreate the observed variations.

We are able to explain the large amplitude seen in the near-IR with two different models. The first has $T_{\rm wd}$ = 65 000 K and the second has $T_{\rm wd}$ = 54 000 K. The difference is the value of the bolometric reflection albedo (w) used for the secondary star. As discussed in HC16, normally, for late-type convective stars, the bolometric reflection albedo is $w = 0.5$. However, Barman, Hauschildt & Allard (2004) found that the intense irradiation of a cool star by a hot white dwarf should result in a dramatic change to its bolometric reflection albedo such that it should be like those of radiative stars ($w \simeq 1$). Barman et al. found that for a situation similar to that for V1500 Cyg, the bolometric albedo should be closer to $w = 0.8$. With this value of w, the large amplitude of the *JHK* light curves can be reproduced with the lower temperature white dwarf. Note that we can also increase the light-curve amplitude by increasing the orbital inclination. This would reduce the required white dwarf temperature in either scenario. However, we have started at $i = 60^\circ$, and thus have little room to increase the inclination before eclipses begin at $i \geq 72^\circ$. Models with $w = 0.5$, $i = 71^\circ$ and $T_{\rm wd}$ = 60 000 K can reproduce the *BVRIJHK* data set.

The final model light curves presented in Figs 4 and 5 have the temperature of the white dwarf as $T_{\rm eff}$ = 54 000 K and the temperature of the hotspot associated with the primary pole of $T_{\rm eff}$ = 432 000 K. A radius for the hotspot of $R_1 = 28^\circ$ was found to best fit the *B*-band light curve. The WD2010 code will not allow for a much hotter temperature spot than this (the limit is 500 000 K), so to get significant optical emission and irradiation requires a sizeable spot radius. The resulting light-curve models explain the rise to maximum in the *BVRI* light curves, but leave significant excesses that peak near $\phi = 0.5$. This model almost fully explains the *JHK* light curves (Fig. 5) from $\phi = 0.9$ to 0.4.

If we again assume that the secondary accretion region is truly located exactly opposite to the primary pole, it would have β_2 = 51°. We do not have a hotspot at this location in the model, as it appeared to contribute little to the X-ray light curve. If the spot is geometrically small, with a radius of ∼3°, it would be visible for nearly 80 per cent of the orbit. Obviously, if the hotspot associated with the secondary accretion region was as large as the primary accretion region, some portion of the secondary hotspot would always be visible. As noted earlier, the southerly latitude of the primary pole means that it is only visible for a smaller part of the orbit. We can delineate the transit duration of each of the two accretion regions in the light-curve plots (magenta and cyan arrows in the *B*-band panel, and corresponding dotted vertical lines) assuming these spot locations. For Figs 4 and 5, we have assumed that the hotspot radius associated with the secondary pole is $R_2 = 3^\circ$, and that for the primary is $R_1 = 28^\circ$.

Due to their simplicity, we examine the new models for the *JHK* light curves first. It is apparent that the largest excess in these light curves is associated with the visibility of the primary pole. There also appears to be evidence for smaller excesses from ϕ = 0.95 to 0.32, and from ϕ = 0.5 to 0.7. Those excesses must be associated with the secondary accretion region. The drop in the flux in each of the three bandpasses after $\phi = 0.7$ suggests that the cyclotron emission at this time is rapidly declining. The optical spectra, however, show that there is significant cyclotron emission from the primary pole at $\phi = 0.94$. Given the inherent variability of cyclotron emission, as demonstrated in the two sets of *JHK* light curves in HC16 (their figs 7 and 8), perhaps the accretion rate simply declined as the system approached $\phi = 1.0$ at the epoch of the infrared observations. The more likely explanation, however, is

[2] ftp.astro.ufl.edu/pub/wilson/lcdc2010/

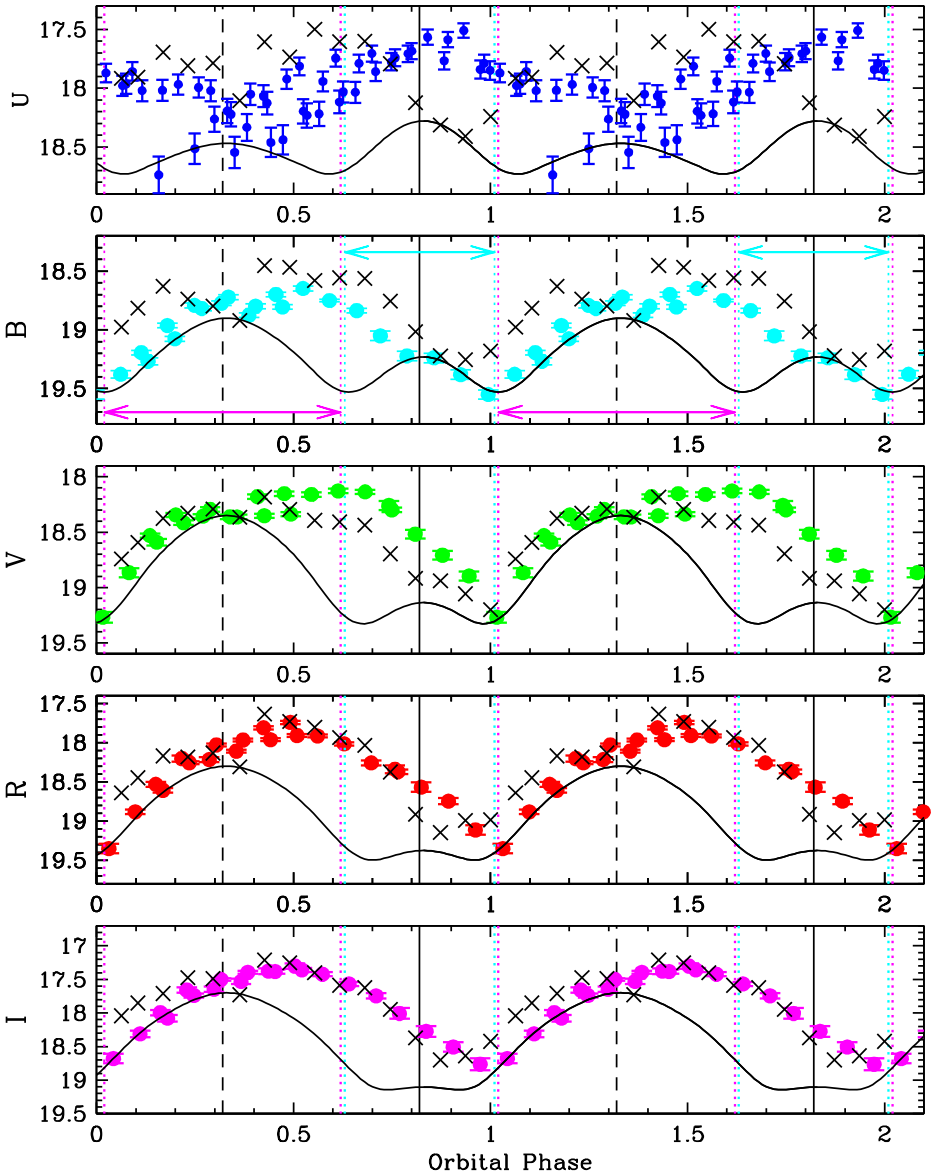

Figure 4. The *UBVRI* light curves of V1500 Cyg for 2014 August 31 (from HC16). The black crosses represent the photometry derived from the new spectroscopy. The vertical solid line is the phase of the transit of the primary X-ray pole, while the dashed line is the transit of the secondary pole. The dotted cyan lines and arrows (in the *B*-band panel) indicate the phases that the primary X-ray pole is visible, while the magenta dotted lines and arrows are for the secondary pole. The solid black curve is the light-curve model described in the text.

that there is cyclotron emission from the secondary pole throughout most of the orbit, and the model light curves need to be shifted downwards by $\gtrsim$0.2 mag. This conclusion is directly supported by the models to the spectra that show that cyclotron emission from the 105 MG field is present from $\phi = 0.0$ to 0.75.

For the two fields used to model the cyclotron emission above, any near-IR emission must come from the cyclotron fundamentals. The cyclotron fundamental is very broad at the high temperatures and values of logΛ found in the two sets of models. For the 72 MG field model at $\phi = 0.87$, the $n = 1$ harmonic has its peak flux near 1.35 μm. For the 105 MG field, the cyclotron fundamental peaks near 9500 Å. As discussed in Harrison & Campbell (2015), unlike the higher harmonics, the cyclotron fundamental has its peak emission at low viewing angles (see their fig. 6). It is interesting that all three light curves show a small peak right at the time of transit of the secondary pole. There is also an inflection in the *H*- and *K*-band light curves at the time of the primary pole transit. The photometric excesses observed in the near-IR appear to be completely consistent with a cyclotron interpretation.

Comparison of the models to the optical light curves shows that the largest excesses occur in the phase interval $\phi = 0.32$ to 1.0. For the photometry shown in Fig. 4 for 2014 August 31, the peak in the *BVRI* light curves occurred at a time when both poles were visible. A similar result is found from the spectroscopically derived light curves. Except for the *V*-band light curve, the spectroscopic photometry is very similar to the photometric light curve. The deviation of the *V* band is easily explained due to the fact that the truncated bandpass only captures a fraction of the flux from the dominant harmonics of either field.

The light-curve model for the *B* band clearly shows the presence of the hotspot region associated with the primary X-ray pole. Due to its extreme temperature, it has little influence on the data beyond

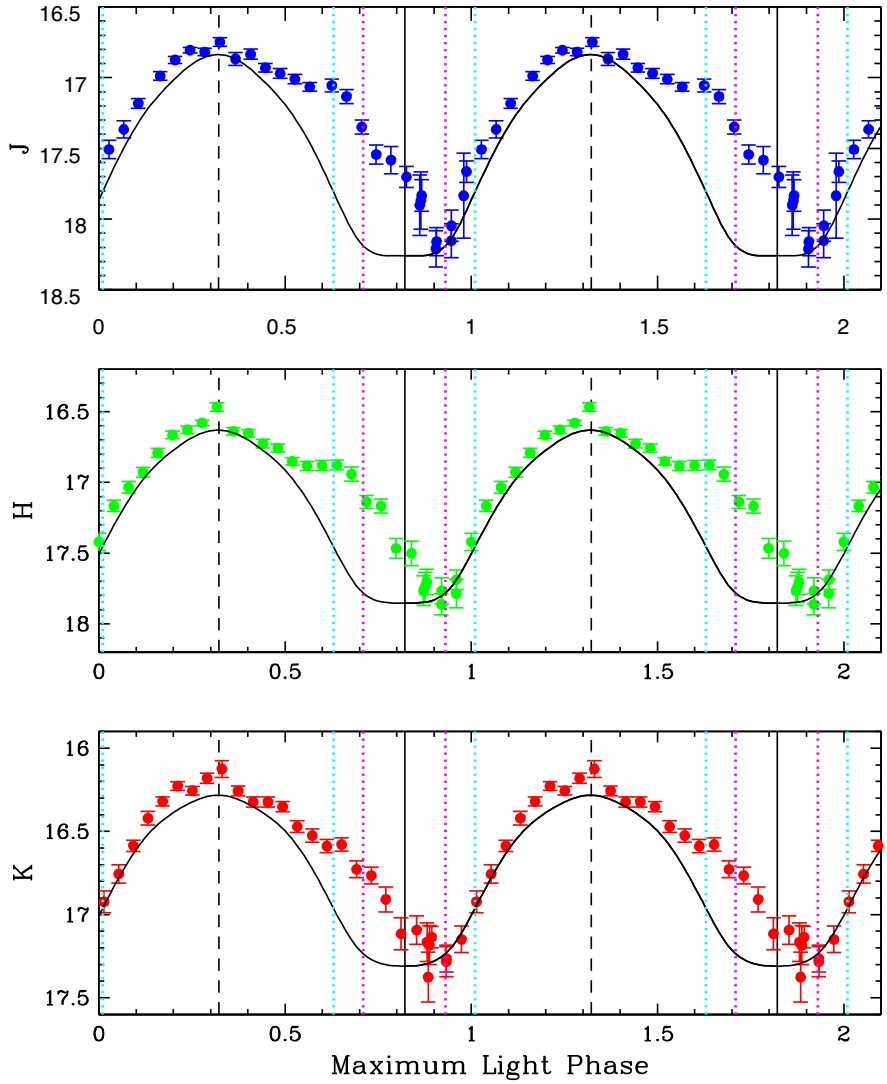

Figure 5. The *JHK* light curves of V1500 Cyg for 2014 October 30 (from HC16), as in Fig. 4. The dashed, dotted and solid lines are as those in Fig. 4.

the *V* band. It is guaranteed that much of the excess that we have wholly attributed to the hotspot in the *B* band arises from cyclotron emission from the primary pole, and that this hotspot is actually smaller than we have assumed here. The spectroscopic light curves in *V*, *R* and *I* all show a small dip at $\phi = 0.82$, relative to the photometric data. In contrast, the spectroscopic *BVRI* light curves from phase 0 to phase 0.2 show an excess above the photometric light curves. This type of variability is common among magnetic cataclysmic variables, but the constancy of the phasing of the light curves, and their excesses, is further support for a synchronized system.

The *U*-band light curve that was difficult to understand using the old binary phasing now appears to be more comprehensible. As discussed in HC16, there are times when the flux in this bandpass suddenly drops to very low levels. These minima allow us to set the floor for the two-component light-curve model. The maximum in the *U*-band photometry now occurs close to the time of the transit of the primary X-ray emission region, with its associated hotspot. While some of the excess emission in this bandpass is probably due to the H I Balmer continuum, it is important to stress that the $n = 3$ harmonic for the 105 MG field peaks near 3500 Å. Unfortunately, our spectra do not go far enough bluewards to fully appreciate its contribution. This harmonic, however, supplies much of the flux shortwards of 4500 Å for the spectra in Fig. 2(b). Given this fact, and the presence of the $n = 4$ harmonic of the $B = 72$ MG field in the *U* band, the strong excesses above the light-curve model throughout the orbit can be directly attributed to cyclotron emission.

While the spectroscopic *U*-band light curve is consistent with the data from *XMM* for most of the orbit, right near the time of the transit of the primary pole, there was a sudden drop in flux. This might be due to the red bias of the synthetic *U* band. This dip, however, is mirrored in the *VRI* light curves. Perhaps the cyclotron emission at the epoch of the spectroscopy was weaker than it was at the time of the photometry. The fact that the cyclotron emission from the primary pole was still present in the spectra at these phases provides additional support for a small offset of the model light curves to fainter magnitudes.

4 DISCUSSION

The analysis of the *XMM* observations in HC16 was surprising, suggesting that the asynchronous polar V1500 Cyg had attained synchrony much earlier than predicted. It had reverted to being a synchronous polar. The optical and infrared light curves obtained

at various epochs over the past decade also supported the interpretation of a synchronous system: the main excesses/distortions in these light curves repeated at the same phases. If V1500 Cyg was now a synchronous polar, the strong light-curve excesses suggested that emission from discrete cyclotron humps *could* be visible. We have obtained phase-resolved spectra of V1500 Cyg that show such features, and they change in size and shape over the orbit like the cyclotron features seen in other polars. The *BVRIJHK* light-curve analysis in HC16 estimated field strengths for the two cyclotron emission regions of ∼80 and ≥120 MG. Our new modelling of the spectra finds $B_1 = 72$ MG and $B_2 \simeq 105$ MG. The breadth of the cyclotron humps from the primary pole leads to a temperature that is consistent with that derived from the *XMM* data set. We find, however, that to explain the profile of the cyclotron humps from the secondary pole requires a much hotter temperature than indicated by the X-ray observations. Unfortunately, the complexity of the light curve from the underlying binary, combined with the coarse phase resolution and modest S/N of our data set, limits our ability to accurately constrain the properties of the cyclotron emission regions. This is especially true for the secondary pole. To achieve more robust results for *both* poles will require better constraints on the cyclotron emission from the secondary pole, since emission from this pole appears to be present at some level for nearly the entire orbit.

HC16 found it to be extremely difficult to attribute the excesses in the light curves of V1500 Cyg to cyclotron emission if the phase of the *V*-band maximum at $\phi = 0.5$ was superior conjunction of the donor. They required large offsets of the cyclotron emission regions from the X-ray poles, and bent field lines, to produce the observed modulations. If we shift the time of superior conjunction to correspond to the transit of the secondary pole, $\phi = 0.32$, the photometric excesses are easily explained. The largest excesses in the visual data occur during phases when both poles are visible.

While the new phasing of the light curves leads to photometric excesses that are now consistent with the locations of the two X-ray poles, this is not as true for the spectra. The main issues occur near phase $\phi = 0.7$, and between phases 0.94 and 0.17. Given our limited ability to constrain the location of the secondary pole, the period of its visibility remains difficult to quantify. Using a very small spot radius for this pole suggests that it would become self-eclipsed near $\phi = 0.71$. It appears that this event actually occurs closer to $\phi = 0.62$. However, by $\phi = 0.68$, cyclotron emission that we associated with this pole is again present! It does not fully disappear until after $\phi = 0.75$. One simple explanation for this behaviour is that it is not located exactly opposite to the primary pole. Comparison of the spectroscopically derived light curves to the photometric light curves during this phase interval shows that they are quite similar, and thus the change in the morphology of the spectra seen at these phases does not appear to be atypical.

The emergence of the cyclotron humps from the primary pole near $\phi = 0.75$ is later than expected given the phasing of the X-ray pole. The self-eclipse of this region should occur near $\phi = 0.0$. While the cyclotron emission from this pole *does* disappear at this phase, it returns at $\phi = 0.06$ and appears to remain visible up to $\phi \simeq 0.17$. The only explanation we can come up with is that the cyclotron emission region associated with the primary pole is offset by about +0.15 in phase. This localization would mean that it rises and sets later than predicted. The disappearance of the cyclotron emission from this pole at $\phi = 0.0$ might be attributable to the transit of the emission region across our line of sight. Rapid declines in the cyclotron emission can occur when we look down the accretion funnel (see Bailey et al. 1982). In this geometry, we are looking along the accretion stream, and this material can obscure our line of sight to the cyclotron emission region. The H I emission lines are at their weakest near $\phi = 0$, which is also consistent with such an event (see Howell et al. 2008). Additionally, the low values for $\log\Lambda$ that we found in modelling the emission from the primary pole also suggest that this region is offset from the X-ray pole. Given the large accretion rate, and high temperatures implied by the X-ray data, one would expect the main shock region to have very high optical depth. This was not found in our modelling.

5 CONCLUSIONS

Given that (1) we know of no asynchronous polars whose spectra show discrete cyclotron harmonic features, (2) we have an X-ray data set that suggests a spin period similar to the orbital period and (3) a relatively consistent photometric behaviour that can be fully explained by the observed cyclotron emission, we conclude that V1500 Cyg has again become a synchronous polar, well ahead of expectations. As noted in the introduction, Campbell & Schwope (1999) developed a model that relied on a torque on the white dwarf that resulted from the currents and electric fields induced in the secondary by the asynchronous rotation of the magnetic primary to estimate the spin-down time-scale of the white dwarf in V1500 Cyg. Our data set suggests that synchrony occurred within ∼32 yr of the CN eruption. Using the Campbell & Schwope formulation, if the white dwarf mass in V1500 Cyg is 1.0 $M_\odot$, and the magnetic field strength is 40 MG, the spin-down time would be 110 yr. However, the synchronization time-scale is dependent on B^{-2}. Using $B = 72$ MG, the time-scale for synchronization of the white dwarf in V1500 Cyg is only 34 yr. With all of the uncertainties that go into this estimate, the result is remarkable.

To fully understand V1500 Cyg will require additional epochs of spectroscopy. Data obtained on a larger telescope are necessary to both improve the S/N ratio and provide better phase resolution. There might also be epochs when the cyclotron emission from the secondary accretion region is much stronger than what we observed. If so, it might be possible to develop more robust cyclotron models for this pole. It would also be interesting to obtain new phase-resolved near-IR spectroscopy to search for emission from the cyclotron fundamentals. We re-examined the *JHK* spectra presented in Harrison, Campbell & Lyke (2013, obtained with NIRC on Keck in 2006), but could not find any evidence to support the presence of discrete cyclotron harmonic features in those data.

ACKNOWLEDGEMENTS

This paper is based on observations obtained with the Apache Point Observatory 3.5 m telescope, which is owned and operated by the Astrophysical Research Consortium. We thank the anonymous referee for useful comments.

REFERENCES

Bailey J., Hough J. H., Axon D. J., Gatley I., Lee T. J., Berriman G., Szkody P., Stokes G., 1982, MNRAS, 199, 801
Barman T. S., Hauschildt P. H., Allard F., 2004, ApJ, 614, 338
Bessell M. S., 1991, AJ, 101, 662
Bessell M. S., 1999, PASP, 111, 1426
Campbell R. K., 2008, PhD thesis, New Mexico State University
Campbell C. G., Schwope A. D., 1999, A&A, 343, 132
Cardelli J. A., Clayton G. C., Mathis J. S., 1989, ApJ, 345, 245
Cheselka M., Holberg J. B., Watkins R., Collins J., 1993, AJ, 106, 2365

Collazzi A. C., Schaefer B. E., Xiao L., Pagnota A., Kroll P., Löchel K., Henden A. A., 2009, AJ, 138, 1846
Harrison T. E., 2016, ApJ, 833, 14
Harrison T. E., Campbell R. D., 2015, ApJS, 219, 32
Harrison T. E., Campbell R. D., 2016, MNRAS, 459, 4161 (HC16)
Harrison T. E., Campbell R. D., Lyke J. E., 2013, AJ, 146, 37
Howell S. B., Harrison T. E., Szkody P., Walter F. M., Harbeck D., 2008. AJ, 136, 2541
Lance C. M., McCall M. L., Uomoto A. K., 1988, ApJS, 66, 151
Politano M., Starrfield S., Truran J. W., Weiss A., Sparks W. M., 1995, ApJ, 448, 807
Schmidt G. D., Stockman H. S., 1991, ApJ, 371, 749
Schmidt G. D., Liebert J., Stockman H. S., 1995, ApJ, 441, 414
Schwope A. D., 1990, Rev. Mod. Astron., 3, 44
Schwope A. D., Beuermann K., 1997, Astron. Nachr., 318, 111
Semeniuk I., Olech A., Nalezyty M., 1995, Acta Astron., 45, 747
Slavin A. J., O'Brien T. J., Dunlop J. S., 1995, MNRAS, 276, 353
Stockman H. S., Schmidt G. D., Lamb D. Q., 1988, ApJ, 332, 282
Vennes S., Thejll P. A., Genova Galvan R., Dupuis J., 1997, ApJ, 480, 714

This paper has been typeset from a TEX/LATEX file prepared by the author.